The structure of Staphylococcus aureus epidermolytic toxin A, an atypic serine protease, at 1.7 Å resolution

Jean Cavarelli, Gilles Prévost, William Bourguet, Luc Moulinier, Bernard Chevrier, Bénédicte Delagoutte, Alexandrine Bilwes, Lionel Mourey, Samer Rifai, Yves Piémont, et al.

▶ **To cite this version:**

Jean Cavarelli, Gilles Prévost, William Bourguet, Luc Moulinier, Bernard Chevrier, et al.. The structure of Staphylococcus aureus epidermolytic toxin A, an atypic serine protease, at 1.7 Å resolution. Structure, 1997, 5 (6), pp.813-824. 10.1016/s0969-2126(97)00235-9 . hal-03004650

HAL Id: hal-03004650
https://cnrs.hal.science/hal-03004650

Submitted on 20 Nov 2020

HAL is a multi-disciplinary open access archive for the deposit and dissemination of scientific research documents, whether they are published or not. The documents may come from teaching and research institutions in France or abroad, or from public or private research centers.

L'archive ouverte pluridisciplinaire **HAL**, est destinée au dépôt et à la diffusion de documents scientifiques de niveau recherche, publiés ou non, émanant des établissements d'enseignement et de recherche français ou étrangers, des laboratoires publics ou privés.

The structure of *Staphylococcus aureus* epidermolytic toxin A, an atypic serine protease, at 1.7 Å resolution

Jean Cavarelli[1*], Gilles Prévost[2], William Bourguet[1], Luc Moulinier[1], Bernard Chevrier[1], Bénédicte Delagoutte[1], Alexandrine Bilwes[1†], Lionel Mourey[1‡], Samer Rifai[2], Yves Piémont[2] and Dino Moras[1]

Background: Staphylococcal epidermolytic toxins A and B (ETA and ETB) are responsible for the staphylococcal scalded skin syndrome of newborn and young infants; this condition can appear just a few hours after birth. These toxins cause the disorganization and disruption of the region between the *stratum spinosum* and the *stratum granulosum*—two of the three cellular layers constituting the epidermis. The physiological substrate of ETA is not known and, consequently, its mode of action *in vivo* remains an unanswered question. Determination of the structure of ETA and its comparison with other serine proteases may reveal insights into ETA's catalytic mechanism.

Results: The crystal structure of staphylococcal ETA has been determined by multiple isomorphous replacement and refined at 1.7 Å resolution with a crystallographic R factor of 0.184. The structure of ETA reveals it to be a new and unique member of the trypsin-like serine protease family. In contrast to other serine protease folds, ETA can be characterized by ETA-specific surface loops, a lack of cysteine bridges, an oxyanion hole which is not preformed, an S1 specific pocket designed for a negatively charged amino acid and an ETA-specific N-terminal helix which is shown to be crucial for substrate hydrolysis.

Conclusions: Despite very low sequence homology between ETA and other trypsin-like serine proteases, the ETA crystal structure, together with biochemical data and site-directed mutagenesis studies, strongly confirms the classification of ETA in the Glu-endopeptidase family. Direct links can be made between the protease architecture of ETA and its biological activity.

Addresses: [1]Institut de Génétique et de Biologie Moléculaire et Cellulaire, CNRS/INSERM/ULP, BP 163, 67404 Illkirch Cedex, France and [2]Institut de Bactériologie de la Faculté de Médecine, 3 rue Koeberlé, 67000 Strasbourg, France.

Present addresses: [†]The Salt Lake Institute, 10010, North Torrey Pines Rd, La Jolla, CA 92037, USA and [‡]Groupe de Cristallographie Biologique, IPBS/CNRS, 205 route de Narbonne, 31077 Toulouse Cedex, France.

*Corresponding author.
E mail: cava@igbmc.u-strasbg.fr

Key words: epidermolytic toxin, serine hydrolase, serine protease, *Staphylococcus aureus*, X-ray diffraction

Received: 11 February 1997
Revisions requested: 11 March 1997
Revisions received: 14 April 1997
Accepted: 8 May 1997

Structure 15 June 1997, 5:813–824
http://biomednet.com/elecref/0969212600500813

© Current Biology Ltd ISSN 0969-2126

Introduction

Epidermolytic or exfoliative toxins (ETs) are protein toxins secreted by *Staphylococcus aureus*. These toxins are responsible for the staphylococcal scalded skin syndrome (SSSS) or *impetigo contagiosa* [1–3], which is primarily observed in newborn and young infants. Babies are rarely infected with ET-producing *S. aureus* at birth, but newborns may acquire the staphylococci from healthy nasal carriers, such as nurses. If skin infection by these toxigenic staphylococci occurs, newborns develop the typical SSSS, which results in splitting between the *stratum spinosum* and the *stratum granulosum*—two of the cellular layers constituting the human epidermis [4]. Such lesions may be at the origin of systemic infections [5], because desquamation will expose the infant to various bacterial infections that could lead to septicemia. Outbreaks of SSSS are not uncommon in newborn care units [6]. A few cases of SSSS in immunocompetent adults [7] and HIV-1 seropositive patients have also been reported [8]. Experimental SSSS can be obtained after subcutaneous injection in newborn mice. They show splitting and loss of elasticity within epidermis, which is called the Nikolsky's sign [2].

Two serotypes of ETs, called ETA and ETB, have been identified and purified [9,10], and their genes have been sequenced [11,12]. Native exfoliative toxins mature from a longer precursor protein, which is proteolytically cleaved of a signal peptide during the secretion process. This signal peptide contains a sequence of positively charged amino acid residues followed by hydrophobic residues. The proteolytic cleavage occurs after an alanine residue, as is the case with most of the staphylococcal exotoxins. The ETA precursor contains 280 amino acids, whereas the mature protein contains 242 residues. Secreted ETA and ETB share 55% sequence identity; they are chromosome- and plasmid-encoded, respectively [12]. ETs are secreted by about 5% of *S. aureus* strains isolated from patients with SSSS [13]. Two other types of exfoliative toxins have been reported—one from *S. aureus* [14] and the other from *Staphylococcus hyicus* [15], but their sequences remain unknown.

Initially, ETs were thought to be proteases because of the caseinolytic activity (cysteine protease activity) of purified ET fractions [16]. The results presented here show that this observation was probably due to a protein contamination during purification. Sequence analysis revealed homology between ETs and serine proteases [17,18], however, such as between the staphylococcal V8 protease and a protease from *Streptomyces griseus*, Glu-SGP, both of which are specific for a glutamate residue. ET sequences include the conserved catalytic triad, Ser195(195), His72(57) and Asp120(102), which is common to serine proteases, esterases and lipases. (Primary sequence numbers refer to the linear sequence of the mature protein. Residue numbers in parentheses refer to topological equivalences in the classical nomenclature of trypsin-like serine proteases.). Furthermore, the functional role of Ser195(195) was confirmed by site-directed mutagenesis. Substitutions of Ser195(195) by glycine or cysteine resulted in biologically inactive toxins when tested on the newborn mouse skin model [19,20]. The physiological target of ETs is unknown, and, despite numerous assays with chromogenic peptide substrates, no enzymatic activity has been evidenced [20]. No marked sequence similarity was found between the ETs and a glutamic-acid-specific endopeptidase from *S. aureus* [21]. However, an esterolytic activity with quite poor kinetic constants was found for both ETA and ETB with the Boc–L-Glu–OPhenyl synthetic substrate [17].

ETs were also suspected of being superantigens [22]. They activate Vβ2+ (and to a lesser extent Vβ2–) human T-lymphocytes and, thus, cause an increase in expression of cutaneous T-lymphocyte-associated antigen [23]. Although it is not known whether the latter is a direct effect, or the result of cascade events.

Results and discussion

Structure determination

ETA crystals belong to space group $P2_1$ with unit cell dimensions a = 49.09 Å, b = 66.40 Å, c = 81.77 Å, β = 93.92°, and they diffract to a resolution limit better than 1.7 Å at a synchrotron source. A native Patterson map gave a strong peak (35% of the origin peak) at relative coordinates (x = 0.40, y = 0, z = 0.5) which was interpreted as a noncrystallographic translation vector between two molecules in the asymmetric unit cell, corresponding to Vm = 2.46 Å^3/Da. Heavy-atom derivatives were prepared to solve the phase problem, but only 2 out of 20 heavy-atom derivatives gave significant amplitude differences with native ETA. To overcome this difficulty, two mutated proteins were purified and crystallized in the same space group as wild-type ETA. Initial phases were thus determined using two derivatives of the wild-type protein and three derivatives of the mutants. The data-collection and phasing statistics are given in Table 1. The structure of ETA has been refined at 1.7 Å resolution to a crystallographic R factor of 18.4% (see Table 2 for refinement statistics). The crystallographic asymmetric unit contains 2 molecules each of 242 residues and 417 ordered water molecules. No metal ion binding site is present in the ETA structure.The $2F_o–F_c$ map (with cross-validated Sigmaa-weighted coefficients [24,25]) is of high quality and shows continuous well-defined density for 97% of the amino acids. Seven residues of each monomer have poorly defined electron density (mainly sidechains of exposed lysines or arginines). The model has a good stereochemistry — all residues, except Leu217(220) of each monomer, are in the allowed regions of the Ramachandran diagram (see Table 2). The final structure shows that the two molecules in the asymmetric unit are related by a small rotation of 6.5° around an axis (direction cosines 0.04, 0.97, 0.24) close to the b axis, followed by a translation vector of 18.47 Å, –0.388 Å, 41.04 Å, with a root mean square (rms) deviation between the Cα atoms of the 2 monomers of 0.267 Å (the average displacement of all atoms is 0.196 Å.

A trypsin-like protein fold

In Figure 1, the tertiary structure of ETA is shown as a Cα-backbone trace. The protein contains two domains (I and II) of similar structure, which are built around a six-stranded antiparallel β sheet folded into a β barrel (Fig. 2). This architecture is well-known as the serine protease chymotrypsin-like fold, which has been illustrated by several high resolution structures (recently reviewed in [26,27]). Domain I is composed primarily of residues from Arg38(27) to Asn148(129) and the C-terminal portion of the molecule, Gly228(230)–Glu242(244), contains helix α5 — Asn231(233)–Lys240(242). Domain II is composed primarily of residues from Asp149(130) to Val227(229) and of the N-terminal portion of the molecule, Glu1(1A)–Asp34(23), which contains helix α1, (Ser3(1C)–Gly19(7). The catalytic tetrad, His72(57), Asp120(102), Ser195(195) and Ser211(214), lies at the interface between the two domains.

The ETA structure is very similar to that of the trypsin SGT from *Streptomyces griseus* [28]; this is evident from the rms difference over 123 equivalent Cα atoms which is 1.21 Å (see Fig. 3 for structural alignment and for secondary structure assignments). There are, however, large differences between ETA and the classical trypsin-like serine protease fold in the so-called surface loops — loop A comprises residues 50(34)–56(41), loop B residues 74(59)–84(64), loop C residues 113(91)–119(101), loop D residues 165(145)–167(152), loop 1 residues 187(184)–189(189), loop 2 residues 213(216)–223(225) and loop 3 residues 179(164)–184(181). Among a number of chymotrypsin-like serine proteases, loops A,B,C and D are known to be involved in determining subsite preferences, whereas loops 1,2 and 3 influence the specificity of the S1 site [26]. As in mammalian proteases, the C-terminal helix of ETA packs against the hairpin containing the catalytic

Table 1

Data collection and phasing statistics.

	Data set						
	Native 1	Native 2	Mersa	$KAuCl_4$	EtHgCl	DiHgCl	PCMBS
Protein* (ETA)	wild type	wild type	wild type	wild type	S195C	S195C	S147C
X-ray source	Lure	Lab	Lab	Lab	Lab	Lab	Lab
Wavelength (Å)	0.9	1.5418	1.5418	1.5418	1.5418	1.5418	1.5418
Resolution (Å)	10–1.7	27–3.1	27–3.1	27–3.35	27–2.7	27–2.7	30–3
Number of observations	226 508	46 207	44947	37 400	34 477	39 326	30 277
Number of unique reflections	57 158	9 141	8 542	7508	13 247	13 866	10 816
Completeness (%)	99	95	88	98	91	95	98
1.7 Å–1.8 Å (F/σ > 3)	85						
R_{sym} † (%)							
all range	4.8	5.2	5.5	5.5	7.7	7.1	3.4
1.7 Å–1.73 Å							
(9807 obs/ 2810 reflections)	17.7						
Heavy atom concentration (mM)			4	3	2	2	1
Soaking time (h)			12	24	4	4	1
Number of sites per molecule			4	4	1	2	1
R_{iso} ‡ (%)			15.4	16.1	22.9	20.7	8.4
Phasing power§ (centric–acentric)			0.76–1.1	1.2–1.4	0.81–0.96	1.20–1.35	1.1–1.05
R_{cullis} # (centric–acentric)			0.9–0.92	0.86–0.83	0.90–0.92	0.84–0.83	0.91–0.9

*Proteins used for data collection: wild type; mutant (S195C), where Ser195 has been substituted by Cys; mutant (S147C), where Ser147 has been substituted by Cys. †$R_{sym} = \Sigma_h\Sigma_i |< I_h > - I_{h,i}| / \Sigma_h\Sigma_i I_{h,i}$, where $I_{h,i}$ is the intensity of a measured reflection h and $< I_h >$ is the average intensity for this unique reflection. ‡$R_{iso} = \Sigma h |F_{der} - F_{nat}| / \Sigma_h F_{nat}$, where F_{nat} and F_{der} are the native and derivative structure factor amplitudes. §Phasing power = (root mean square heavy atom structure factor)/(phase integrated lack of closure) (statistics of SHARP). #R_{cullis} = (phase integrated lack of closure)/(root mean square isomorphous difference) (statistics of SHARP). Heavy atoms abbreviations: Mersa (mersalate sodium mersalyl), $KAuCl_4$ (potassium tetrachloro aurate), EtHgCl (chloro ethyl mercury), DiHgCl (1-2 toluidine,-4,6 dimercuriacetate) and PCMBS (p-chloromercuribenzene sulfonate).

Asp120(102) and helps to fix its geometry. In contrast to other serine protease folds, however, ETA is characterized by three unique structural features: firstly, an unusual and inactive conformation of the so-called oxyanion hole; secondly, an additional amphipathic N-terminal helix α1 (Ser3(1C)–Gly19(7)), which interacts with loops 1 and 2; and, thirdly, an absence of cysteine bridges. In all members of the chymotrypsin family of serine proteases, with the exception of the Sindbis virus core protein, three conserved disulfide bonds (C42–C58, C168–C182 and C191–C220, chymotrypsin sequence numbering) connect the short loops. They are probably important for structural stability. None of these bridges are present in ETA.

The presence of two molecules in the asymmetric unit has no biological relevance and is only due to the special packing arrangement. The interfacial area between the two molecules of the asymmetric unit is low — the buried surface area is 426 $Å^2$ per monomer, compared to the overall accessible surface area per monomer of 10 555 $Å^2$. The interactions are mainly water mediated and involve loops A and B of one monomer interacting with loop 2 and the β hairpin (β6–β7) of the other monomer.

The oxyanion hole of ETA is not preformed

Extensive studies on serine proteases have shown that the cleavage of a peptide bond by these enzymes proceeds through a two-step reaction. Each step proceeds through a negatively charged tetrahedral transition state intermediate. In trypsin-like serine proteases, the negative charge developed during the breaking of the scissile bond is usually stabilized in a pocket called the oxyanion hole, by the mainchain atoms of residues located in the vicinity of the catalytic serine. The NH groups of both Gly(193) and Ser(195) play this role in SGT and several other serine proteases.

In the ETA structure, the corresponding peptide, Pro192(192)–Gly193(193), has a unique conformation that has never been observed in serine proteases so far. The CO group of Pro192(192) and the NH group of Gly193(193) point in the opposite directions to those groups in the oxyanion hole of other serine proteases (Fig. 4). In this conformation, the mainchain CO of Pro192(192) makes a hydrogen bond with Oγ of the catalytic Ser195(195) and the mainchain NH group of Gly193(193) hydrogen bonds with Oδ1 of Asp164(144) from loop D. This conformation of the oxyanion hole also implies that His72(57) is protonated, the Nε2 atom making a hydrogen bond with Oγ of the catalytic Ser195(195). In the classical serine protease catalytic scheme, the CO of Pro192(192) could be directed toward the negative charge developed in the tetrahedral transition state, and the NH of Gly193(193) would not be able

Table 2

Refinement statistics.

Refinement program	X-PLOR
Resolution (Å)	8–1.7
Number of reflections ($F > 3\sigma$)	53 177
Number of non-hydrogen proteins atoms (mola, molb)	1905–1905
Number of ordered water molecules	417
R_{model}* (%)	18.4
R_{free}† (%)	23.6
Overall G factor‡ (mola, molb)	0.23–0.25
Average B factors (Å^2)	
all non-hydrogen atoms (mola, molb)	19.6–17.6
mainchain (mola, molb)	17.1–14.9
sidechain (mola, molb)	22.1–20.3
water molecules	39.1
Root mean square deviations from ideal geometry§	
bonds (Å) (mola, molb)	0.005–0.006
angles (°) (mola, molb)	1.241–1.252
torsion(°) (mola, molb)	27.6–27.4
Ramachandran plot quality	
residues in core regions (%) (mola, molb)	89.3–88.8
residues in allowed regions (%) (mola, molb)	9.8–10.7
residues in generous or disallowed regions (%) (mola, molb)	0.5–0.5
Coordinates errors from cross-validated Luzzati plots (Å)	0.21 (0.18, working set)

*$R_{model} = \Sigma_h |F_{obs} - F_{calc}| / \Sigma_h F_{obs}$, where F_{calc} and F_{obs} are the calculated and observed structure factor amplitudes, respectively. †A small fraction (7%) of reflections with no cut-off between 8 Å–1.7 Å (4065 out of 57 140 unique reflections) was excluded from the refinement and used for monitoring the course of the refinement. ‡Overall 'normality' as calculated by PROCHECK [60]. §Root mean square deviations were calculated using Engh and Huber parameters. mola and molb represent the two non-crystallographic molecules in the asymmetric unit.

to stabilize this negative charge. The electron-density map of ETA is of very good quality and does not allow alternative interpretations of this loop (Fig. 5). The tripeptide Pro192(192)–Gly193(193)–Asn194(194) adopts a 3_{10}-helical conformation. The classical stabilization of the developed charge would require a conformational change of this loop, which would only need a rotation of the psi angle of Pro192(192) from one conformationally favorable domain (helical, $\psi = -40°$) to the other one (strand, $\psi = 140°$). This conformational switch should not be energetically expensive—on the basis of free energy simulations of a small polypeptide where a similar conformational change was analyzed [29], the flipping of this bond would cost less than 3 Kcal/mol. Moreover, the residues implicated in this conformational change, namely Asp164(144) of the D loop and Pro192(192)–Gly193(193), are located at the surface of the molecule and no steric constrains should therefore interfere during this local structural switch. One may therefore postulate that a productive oxyanion hole can be formed upon substrate binding.

This unexpected feature of the ETA active site may corroborate a previously unexplained experimental behaviour of our ETA crystals—even at relatively high pressure (20 bars), ETA crystals do not bind Xenon. It has been shown that Xenon binds to several serine proteases in the catalytic site [30], at a site approximately midway between the catalytic serine Ser(195) and the S1 (primary specificity) pocket with very little perturbation of the protein. It was expected that Xenon binding would be a general feature of serine proteases. ETA is the first example of a serine protease that contains an oxyanion hole which is not preformed. Lipases, which possess the same catalytic triad as serine proteases but with a large variation in the chemistry and structure of this triad, also have an oxyanion hole that is not preformed. However, the productive oxyanion hole of lipase is generated by an activation process, induced by a displacement of the protein region that covers the catalytic site which is initially hidden from the protein surface and therefore inaccessible [31–33]. Therefore, the conformational switch necessary

Figure 1

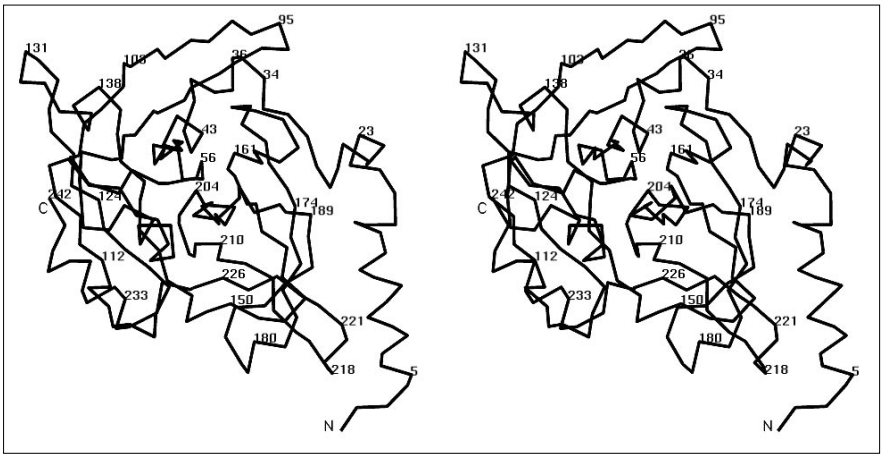

A stereo representation of the ETA Cα backbone. This figure was made with the program SETOR [64]. Numbering is only shown according to the mature sequence of ETA.

for building the oxyanion hole of ETA will be different as the active site is accessible at the protein surface.

An S1 subsite specific for a glutamic acid residue

Looking at ETA from the outside of the molecule toward the catalytic tetrad, and by homology with the other serine proteases, the primary specificity pocket S1 (using the nomenclature introduced by Schechter and Berger [34]) is located at the right-hand side of the molecule (Fig. 2). This pocket is delimited by three polypeptide portions of domain II — loop 1, strands β14 and β15, which flank loop 2, and the N-terminal helix α1. The residues mapping to this region and which should be important for the subsite specificity of ETA are His210(213), Lys213(216), Tyr186 (183) and Thr190(190) (Figs 2, 4).

As predicted by Barbosa *et al.* [35], the ETA S1 pocket may preferentially bind negatively charged substrates that can be stabilized by His210(213). In the back of the pocket, Tyr186(183) is responsible for orienting His210(213). In our crystal structure, a network of water molecules occupies the active site and the entrance of the S1 pocket of ETA, and they link His210(213) to the catalytic triad.

In vitro enzymatic experiments (see below) have shown that ETs hydrolyse a synthetic substrate Boc–L-Glu–OPhenyl, but do not cleave Boc–L-Asp–OPhenyl. Superposition of the ETA structure on that of the glutamic acid serine protease Glu-SGP in complex with a tetrapeptide ligand Boc–Ala–Ala–Pro–Glu–OH [36,37], shows that His213(210) and Ser190(190) of Glu-SGP, which recognize the glutamate moiety of the substrate occupy the same spatial positions as His210(213) and Thr190(190) of ETA (Fig. 6). Therefore, these two residues should play a similar role in substrate binding. The superposition also shows that Lys213(216) of ETA would interact with the sidechain of the glutamate moiety in the S1 pocket. Sequence alignments and structural comparisons of several serine proteases reveal that Lys213(216) is specific for ETs, whereas the other serine proteases have small residues (glycine or serine) at this position (see Fig. 3 for a subset of sequences). In the ETA crystal structure, Lys213(216) also stabilizes the conformation of the S1 pocket by hydrogen-bond interactions with the OH group of Tyr18(8) and the backbone CO atom of Thr190(190). Asn224(226) at the bottom of the S1 pocket could also be a potential candidate for substrate stabilization. Although as this residue is replaced by phenylalanine in ETB, it may only have a structural role.

The ETA-specific amphipathic N-terminal helix

Another characteristic of ETA not seen in other members of the serine protease family is an N-terminal extension of approximately 30 residues. This region adopts an α-helical conformation and packs against domain II. This helix α1 closes one entrance of the S1 subsite and plays a crucial role

Figure 2

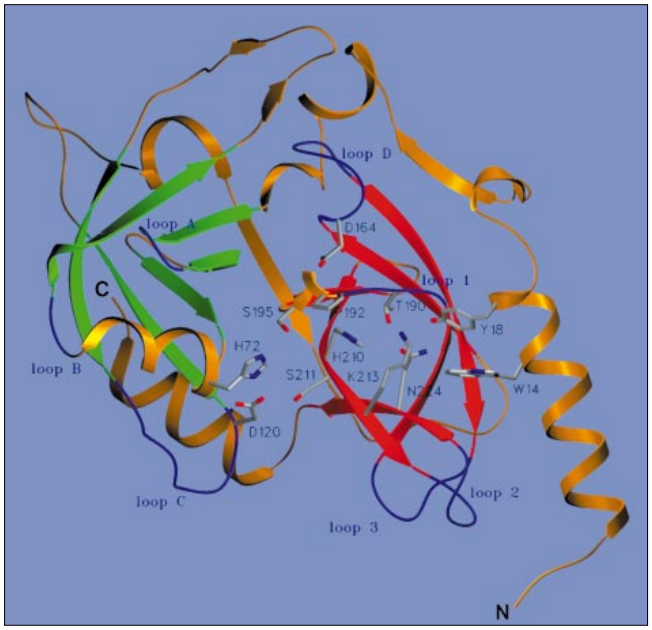

Schematic drawing of the structure of ETA. The two domains, built around a six-stranded antiparallel β sheet characteristic of the trypsin-like serine protease fold, are shown in green for domain I and in red for domain II. The location of the catalytic tetrad, His72(57), Asp120(102), Ser195(195) and Ser211(214), is shown together with the amino acid residues which map the S1 specific pocket. The canonical surface loops [26] (loops A, B, C, D, 1, 2 and 3) are shown in blue. Numbering is only shown according to the mature sequence of ETA.

in its geometry, Tyr18(8) and Trp14(2) being buried in the S1 pocket. Helix α1 is also responsible for the open conformation of loop 2. In all other trypsin-like serine proteases, except for the core protein of Sindbis virus, loop 2 folds back towards the core of domain II, forming a conformation which is partly stabilized by the presence of a disulfide bridge between loop 1 and loop 2. Loop 2 of ETA, that does not contain a cysteine bridge, has an extended conformation which is constrained by several hydrogen-bond interactions with residues belonging to helix α1.

The crucial role of the N-terminal helix of dictating the conformation of the S1 specific pocket and therefore the substrate specificity of ETA has been confirmed by *in vitro* experiments using a synthetic substrate (Boc–L-Glu–OPh), which is hydrolyzed by ETA. Deletion experiments in the N-terminal extremity of ETA result in an inactive protein (see later discussions).

Enzymatic properties of wild-type and mutant ETs

In vitro *enzymatic properties*

Unlike other Glu-endopeptidases, such as the V8 protease that has the highest sequence homology with ETA, ETs do not show any *in vitro* proteolytic activity against insulin,

Figure 3

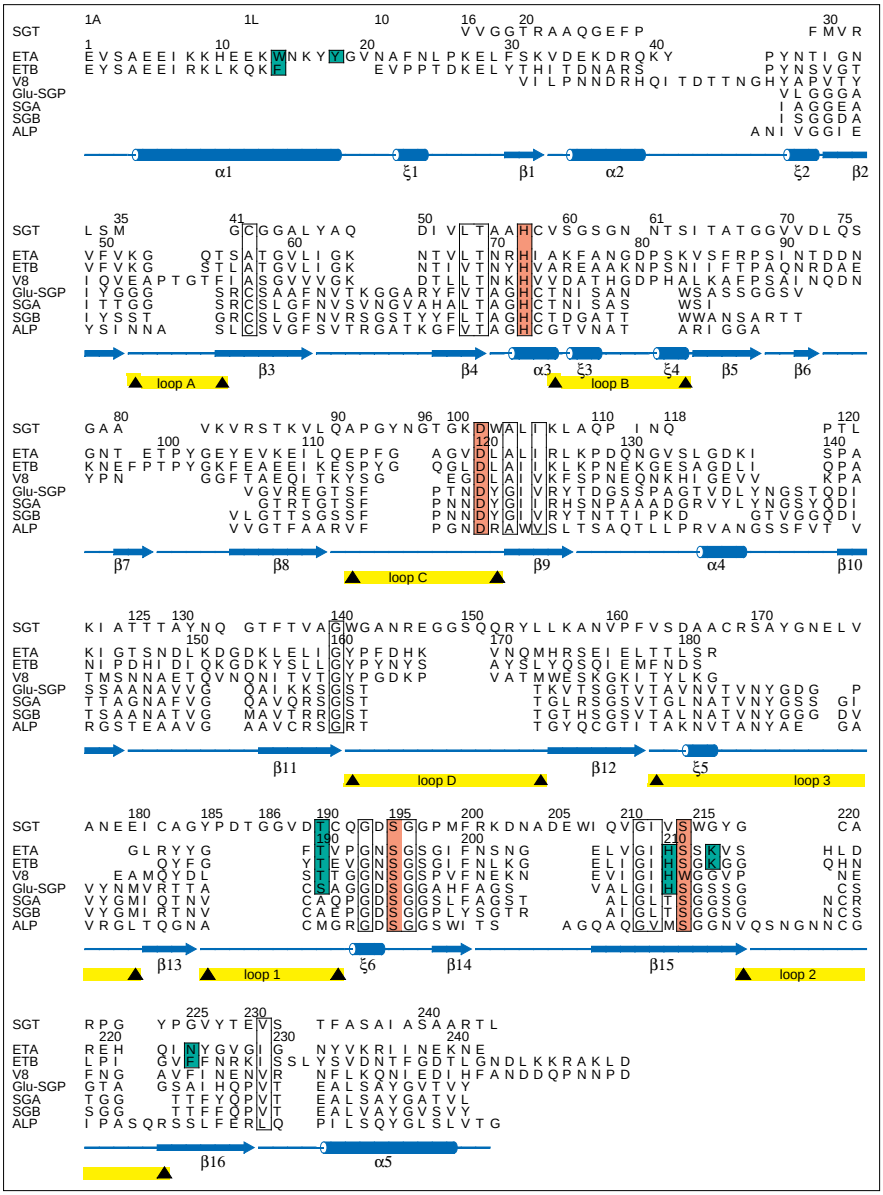

Sequence alignment for ETA, ETB, V8 protease, *S. griseus* trypsin (SGT) [28], *S. griseus* glutamic acid-specific protease (Glu-SGP) [36], *S. griseus* protease A (SGA) [65], *S. Griseus* protease B (SGB) [66] and *Lysobacter enzymogenes* α-lytic protease (ALP) [67]. Amino acid sequence alignment for ETA, SGT, Glu-SGP, SGA, SGB and ALP is based on structure superpositions done with the program WHATIF [61]. The rms deviations after superposition on the ETA structure using atoms differing by less than 2.5 Å are 1.21 Å for SGT (121 atoms used), 1.07 Å for Glu-SGP (73 atoms used), 1.04 Å for SGA (64 atoms used), 1.22 Å for SGB (74 atoms used) and 1.28 Å for ALP (75 atoms used). Secondary structure, determined with program PROMOTIF [68], is also displayed for ETA. Elements of secondary structure are indicated by: α for α helix, β for strand of β sheet, ξ for 3_{10} helix. ETA numbering is shown above the sequence of ETA, whereas canonical trypsin-like serine protease numbering is shown above the sequence of SGT. The residues of the catalytic tetrad are highlighted in orange and the residues of the S1 specific pocket are highlighted in green. The positions of the so-called surface loops (A, B, C, D, 1, 2 and 3) [26], corresponding to those found in the SGT structure are highlighted in yellow. Other residues of similar chemical nature in the aligned sequences (boxed) are either involved in the active site or stabilize the interface between the two domains of the molecule. Asn194(194) and Ser197(197), specific for ETA, ETB and V8 protease, are hydrogen bonded to each other in the ETA structure and stabilize the conformation of the active site. This figure was made with the program ALSCRIPT [69].

casein or bovine serum albumin—proteins which are commonly used as protease substrates *in vitro*. This means either that the natural substrate has multisubsite specificity, or that ETA activity is modulated *in vivo* by another molecule.

Despite observations that ETs did not have any proteolytic activity *in vitro*, Takiuchi *et al.* [16] reported a detectable caseinolytic activity (cysteine protease activity) of ETs, but only when incubated in the presence of crude extract of epidermis of newborn mice. They postulated that the crude extract of the epidermis contains an activating factor of ETA. Our results show that this caseinolytic activity is due to a contamination of ETs by other proteins. We observed that E64, a cysteine protease specific inhibitor, was able to completely inhibit the observed caseinolytic activity (Fig. 7), without modifying the biological activity of ETA on the crude extract of mouse epidermis or its esterolytic activity (data not shown). A new purification procedure of ETA has therefore been developed, which avoids ammonium sulphate precipitation and gives non-contaminated ETA. ETs do not hydrolyze *in vitro* substrates, such as Boc–Ala–Ala–Pro–Glu–*p*-nitroanilide(pNA) and anthranilyl–Ala–Phe–Ala–Phe–Glu–Val–Phe–nitro–Tyr–Asp, some of which are also cleaved by the V8 protease [38].

Although ETA and ETB purified with our current protocol (see Materials and methods) display an esterolytic

Figure 4

Detailed stereo view of the oxyanion hole and the S1 specific pocket of ETA. The location of the catalytic tetrad, His72(57), Asp120(102), Ser195(195) and Ser211(214), and the oxyanion hole, Thr190(190), His 210(213), Lys213(216), Asn 224(226), Tyr186(183), Tyr18(8) and Trp14(2), are shown. Sequence numbering is only shown according to mature ETA.

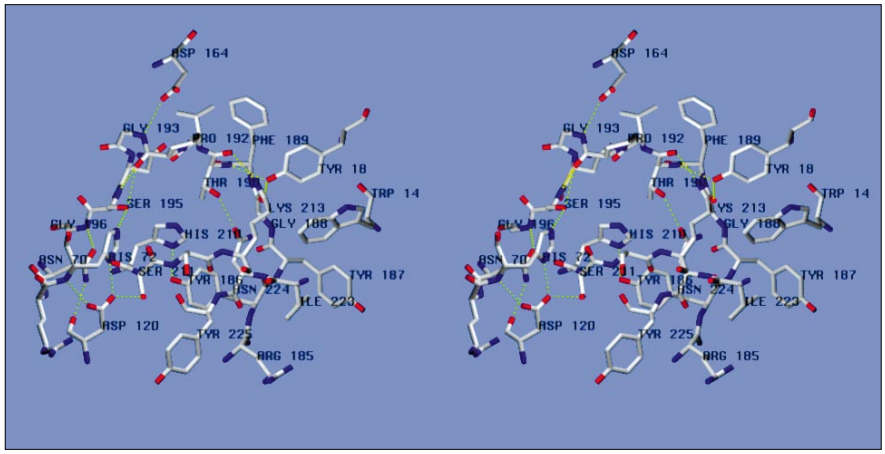

activity when tested with the synthetic substrate Boc–L-Glu–OPhenyl, neither hydrolyze Boc–L-Asp–OPhenyl nor Boc–L-Glu–pNA. These data favor the specificity of the S1 subsite for a glutamic acid; Boc–L-Glu–pNA is not hydrolyzed by ETA due to steric hindrance of the NO2 group by Thr55(40) and Phe76(61) in the S1′ subsite.

The low K_m values for ETA (7.5 mM) and ETB (2.2 mM) observed for Boc–Glu–OPhenyl hydrolysis are in the range of those previously published [17], whereas the specific activity and K_{cat}/K_m values are much higher (Table 3). Amino acid substitutions in ETA of the three residues of the catalytic triad — His72(57), Asp120(102), Ser195(195) — result in a protein with no detectable biological activity *in vitro*. Moreover, deletion of the first ten residues at the N-terminal side (Table 3, ETA ΔGlu1(1A)–His10(1J)) reduced dramatically the kinetic values of the enzyme and deletion of the first twenty residues — the whole helix α1, (Table 3, ETA Glu1(1A)–Val20(9)) produced an enzyme with an undetectable level of activity. These observations further support the role of the N-terminal α-helix in the stabilization of the S1 pocket as observed in the crystal structure. The two deletions in the C-terminal side from Ile236(238) to Glu239(241) also resulted in inactive proteins. This observation can easily be explained by the fact that the C-terminal helix forms a hydrophobic interface with strands β8–β9, containing Asp120(102), and is involved in the stabilization of the active site. Consequently, wild-type ETs cannot be considered as precursors needing further maturation in order to be activated.

In vivo biological activity

Wild-type and mutant ETA described above have been subcutaneously injected into newborn mice. After incubation, the animals were examined in order to observe whether the injected ETA was able to induce the signs of Nikolsky syndrome (Table 3). Unlike wild-type ETs, injection of ETA mutants did not give rise to the characteristic Nikolsky's sign, except for ETA

Figure 5

The active site of ETA. Stereo view of the final ($2F_o–F_c$) cross-validated Sigmaa-weighted map (resolution limits 8 Å–1.7 Å, all data are used, contour level 1σ). Sequence numbering is only shown according to mature ETA.

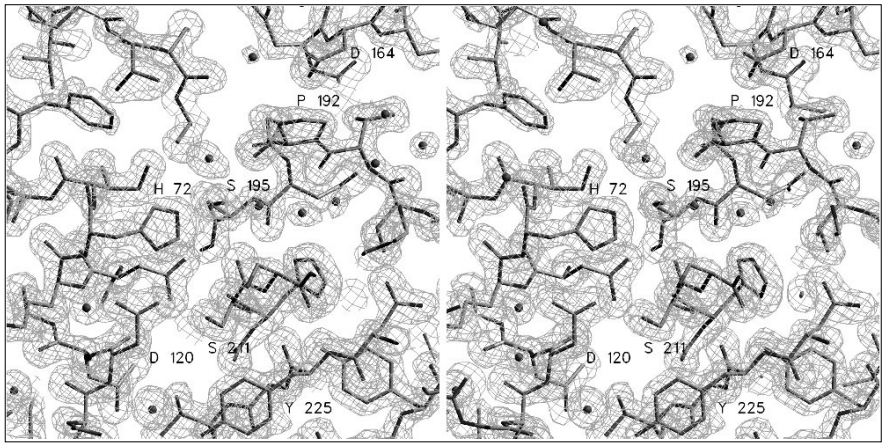

Figure 6

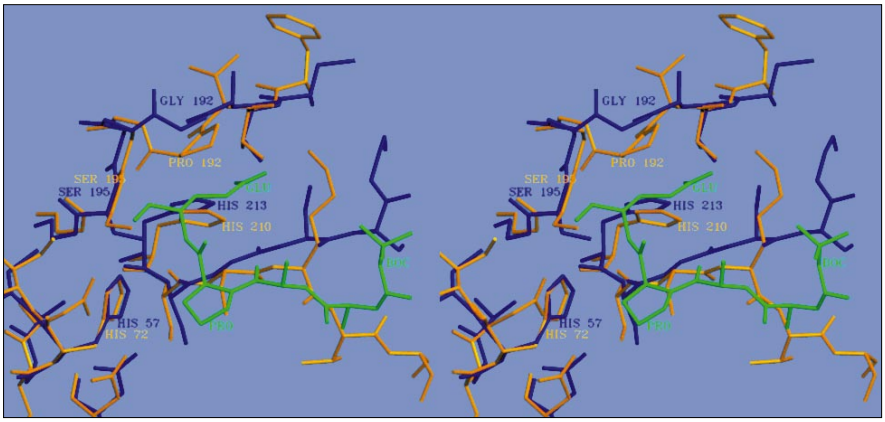

Comparison of the oxyanion hole and the S1 specific pocket of Glu-SGP and ETA. ETA structure together with ETA sequence numbering are shown in gold, whereas Glu-SGP structure together with Glu-SGP sequence numbering are displayed in blue. The Boc–Ala–Ala–Pro–Glu–OH synthetic substrate of Glu-SGP is shown in green. The conformational switch, around Pro192(192) of ETA, necessary for creating a productive oxyanion hole is here clearly illustrated.

ΔGlu1(1A)–Val10(1J) of which a 100 fold higher dose than wild-type ETA was necessary to obtain experimental SSSS. Therefore, there is a very good correlation between *in vitro* enzymatic activity with Boc–L-Glu–OPhenyl substrates and biological capacity of mutant ETA to induce the Nikolsky's sign in newborn mice. These observations are in accordance with the possible hydrolytic activity of ETs in the clinical SSSS.

Biological functions of ETs

The X-ray structure of ETA, together with site-directed mutagenesis experiments, confirms the biological activity of ETA as a serine hydrolase with S1 subsite specificity for a glutamic acid. Mutations of the essential amino acids of the catalytic triad induced the loss of the enzymatic potential, as well as the loss of the functional ability of the toxin to generate the typical splitting of the two epidermal cell layers of newborn mice. ETA may hydrolyze proteins involved in the cell-to-cell attachment in the epidermis. Such proteins would be specific for the interface between two typical cell layers, as shown by cleaving activity experiments in epidermal cell cultures [39]. These specific proteins are expected to disappear almost completely in adults, because it is known that newborns and children are more susceptible to SSSS. Interactions between ETA and these target proteins might result in structural modifications leading to an active form of ETA, as is the case with most serine proteases (upon interaction with coagulation factors or plasmin) involved in precise biological processes. N-terminal or C-terminal processing of the ETA would not occur since ETA activity is sensitive to such deletions.

Figure 7

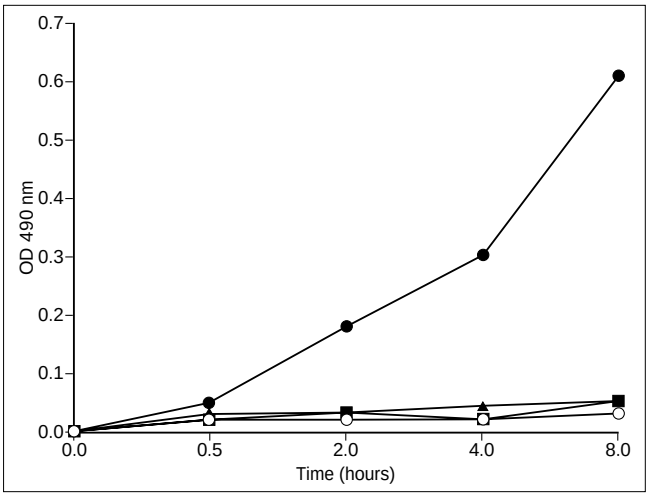

Caseinolytic activities of the previously purified ETA were obtained in the absence of the cysteine-protease inhibitor E64 (solid circle symbol) and disappeared in the presence of E64 (open circle symbol). This activity was monitored by the release of caseine derivative fluorescence-labelled peptide. The highly purified ETA (new protocol presented in this paper) in the absence (solid triangle symbol) or in the presence (solid square symbol) of E64 did not harbour any caseinolytic activity.

The catalytic triad (Asp, His and Ser) is common to proteases, esterases and lipases. Lipases differ from esterases and proteases in being inactive in the absence of a lipid–water interface; this is certainly not the case for ETA. Distinctions between the esterase or protease activity of ETA is not so simple, as it is well known that serine proteases like chymotrypsin also act as esterases.

As the mode of action of ETs on the epidermis is unknown, ETs have also been postulated to be superantigens [40]. The clinical syndrome associated with ET-producing *S. aureus* strains does not evoke a pathology analogous to that provoked by superantigens. Superantigens stimulate cytokine production from lymphocytes, generating fever, hypotension, skin rashes and various disorders in patients. SSSS in newborns may develop rapidly after birth and is only signaled by superficial desquamation without general

Table 3

Esterolytic properties of ETA.

	V_M ($\mu M\,min^{-1}$)	Specific activity ($\mu M\,min^{-1}\,mg^{-1}$)	K_m (mM)	K_{cat}/K_m ($mM^{-1}\,s^{-1}$)	K_{cat} (s^{-1})	Minimal dose## (μg)
*ETA	256.5 ± 40	47.1 ± 8.0	7.5 ± 0.5	2.81 ± 0.07	21.2 ± 3.0	0.5
†ETB	121 ± 9	28.3 ± 1.9	2.2 ± 0.2	5.84 ± 0.11	12.8 ± 0.9	0.5
‡ETA S195C	< 1.0	< 0.5	> 80	> 0.01	> 0.7	> 180
§ETA H72Y	< 1.0	< 0.5	> 80	> 0.01	> 0.7	> 180
#ETA D120T	< 1.0	< 0.5	> 80	> 0.01	> 0.7	> 180
**ETA Δ E1-H10	16 ± 3	2.1 ± 0.4	72 ± 12	0.025 ± 0.005	1.8 ± 0.3	40–50
††ETA Δ E1-V20	< 1.0	< 0.5	> 80	> 0.01	> 0.7	> 180
‡‡ETA Δ I236-E242	< 1.0	< 0.5	> 80	> 0.01	> 0.7	> 180
§§ETA Δ I236-E239	< 1.0	< 0.5	> 80	> 0.01	> 0.7	> 180

In vitro esterolytic properties of ETA for the Boc–L-Glu–OPhenyl synthetic substrate hydrolysis were measured by the release of phenol (monitored at 270 nm). These values were obtained in 0.2 M KH_2PO_4 pH 7.8–1% (v/v) dioxane containing the Boc–L-Glu–OPhenyl compound (0.05–10 mM) at a concentration of 0.17 μM epidermolysins. *Wild-type ETA, †wild type ETB, ‡ETA Ser195(195)Cys mutant, §ETA His72(57)Tyr mutant, #ETA Asp120(102)Thr mutant, **,††ETA truncated at the N-terminal side, ‡‡,§§ETA deleted at the C-terminal side. ##Minimal dose required for observing, *in vivo*, a Nikolsky sign in newborn mice; observations were made 6 h after injection (180 μg represents the limit of protein concentration in 50 μl of physiological solution).

symptoms such as fever, hypotension and T cell proliferation [2]. Experimental cleavage within keratinocyte cell culture was obtained with ETA [39], which suggests no such role for an intermediate cell-like Langerhans cells that represent specialized cells located within the dermis and which are able to promote an immune response. Histological examination of skin with SSSS never mentioned recruitment of immune cells. Superantigen activity is well understood for proteins that interact simultaneously with major histocompatibility complex (MHC) class II molecules on antigen-presenting cells and with the variable parts of the lymphocyte T cell receptor (TCR). Therefore, clinical and experimental observations of SSSS do not account for a superantigen activity of ETs. To date, no hydrolytic activity has been reported from any recognized superantigen. No superantigen activity for ETA was observed by Fleischer *et al.* [41] who carried conventional experiments with purified ETA and also tested a recombinant toxin. Recently, Inoue *et al.* [42] published results on Vβ specificity and expression of a cutaneous lymphocyte-associated (CLA) antigen [23]; they used ETA from a commercial source. No CLA response was observed when testing our purified fractions of ETA and ETB, which remained functional on the animal experimental model (T Zollner, personal communication). The last observation suggests a contamination of purified fractions by known or unknown superantigens, some of which may not have been detectable to date [43]. Such contamination might be of great consequence because superantigens are known to be biologically active at very low concentrations [40].

Biological implications

Staphylococcal epidermolytic toxins A and B (ETA and ETB) are the two protein toxins (ETs) secreted by *S. aureus* that are responsible for the staphylococcal scalded skin syndrome (SSSS) or *impetigo contagiosa* [2], which is observed in newborns and young infants. The secreted forms of ETA (242 amino acid residues) and ETB (245 amino acid residues) have 55% sequence identity and are chromosome- and plasmid-encoded, respectively. They cause disorganization and disruption of the *stratum spinosum* and the *stratum granulosum*—two of the three cellular layers constituting the epidermis. This results in a bullous syndrome with significant desquamation, which exposes infants to various bacterial infections that may lead to septicemia. The SSSS can be reproduced *in vivo* by cutaneous injection of ETA into newborn mice and *in vitro* by addition of ETA to keratinocyte cell cultures. The physiological substrate of ETs is unknown, however, and, consequently, the mode of action of ETs *in vivo* remains an unanswered question. The hydrolytic activity of exfoliative toxins may be exerted on intercellular junctions, which are made up of protein molecules, therefore, the hypothesis of a phospholipase function of exfoliative toxins is not convincing. A superantigen activity for ETs has also been proposed, despite the absence of any clinical observations associated with SSSS resembling a superantigen-induced pathology.

ETA does not cleave *in vitro* any of the proteins that are hydrolyzed by other Glu-endopeptidases. ETA was found to have esterolytic activity against a synthetic substrate Boc–L-Glu–OPhenyl only. Site-directed mutagenesis has shown that ETA mutants defective for this esterolytic activity *in vitro* were also unable to induce experimental SSSS when cutaneously injected into newborn mice.

The crystal structure of ETA has been determined by multiple isomorphous replacement and refined to a high resolution (1.7 Å). Sequence alignments reveal weak

homologies between the staphylococcal V8 protease and ETs, but show that ETs contain the catalytic triad (Ser, Asp and His) common to proteases, esterases and lipases. Mutations of any of the amino acids of the catalytic triad lead to an inactive protein. Despite a very weak sequence homology between ETA and the trypsin-like proteases, ETA displays the well-known fold characteristic of such proteases—containing two domains of similar structure, which are built around a six-stranded antiparallel β sheet folded into a β barrel. The interface of the two domains contains the conserved catalytic tetrad—His72(57), Asp120(102), Ser195(195) and Ser211(214). The S1 subsite is specific for binding a negatively charged substrate, particularly, a glutamic acid. The S1 subsite has characteristics found in other Glu-endopeptidases, nevertheless, the ETA structure reveals new and unexpected features. Firstly, there are large differences in the conformation of ETA's surface loops that decorate the two-barrel structure, especially loop 2 which has an uncommon extended conformation. Secondly, the putative oxyanion hole, which is involved in the stabilization of the tetrahedral transition states of the proteolytic reaction, has an unusual and inactive conformation requiring a molecular switch with low energy cost for activity. Thirdly, disulfide bridges, which are conserved in chymotrypsin-like serine protease and are suspected to be important for either structural stability or active-site stabilization are not present in ETA. And finally, ETA possesses an additional N-terminal extension of 20 residues which folds into an amphipathic helix. The crystal structure shows that this helix is important for ETA biological activity, as it stabilizes the S1 specific subsite; this is confirmed by the biological inactivity of mutants truncated at the N-terminal end. Together with site-directed mutagenesis, the structure of ETA gives a strong argument in favour of the classification of ETA in the serine protease subfamily of proteins that cleave preferentially after a negatively charged residue, namely a glutamic acid. In order to assess such a specific activity, it would be convenient to use labeled biologically active mutants and to check the binding of ETA at the surface of keratinocyte cells. Covalent binding or two-dimensional electrophoresis would be instrumental in characterizing the target molecules of staphylococcal epidermolysins.

Materials and methods

Purification of exfoliative toxin A

S. aureus strain IBS-SA417 (Institut de Bactériologie de Strasbourg *S. aureus*) or recombinant strain 8325-4, which contains mutated genes, were grown at 37°C under an atmosphere containing 10% CO_2 (150× rpm) in 2l Erlenmeyer flasks filled with 1l of 2×TY. Culture was filtered (Ø = 0.45μm) on Pellicon cassette system (Millipore) and the supernatant was further concentrated (cutoff 10 000 Da) to 1l before being dialyzed against H_2O at +4°C. The solution (pH = 5.0) was applied to a SP Fast Flow column® (Pharmacia, Uppsala, Sweden). Proteins that were eluted with a discontinuous gradient of 90 mM $NaCH_3COO$ pH 5.0 (buffer 1; NaCl gradient 600 mM) were then dialyzed against buffer 1 and chromatographed on a MonoS® FPLC (Pharmacia) using a NaCl gradient (0–300 mM) in buffer 1. ETs fractions (180 mM) were pooled and adjusted to 2 M $(NH_4)_2SO_4$ before being applied to an alkyl-Superose® FPLC (Pharmacia) and eluted in a $(NH_4)_2SO_4$ gradient (2–0 M) in 50 mM KH_2PO_4 pH 7.0. ETs eluted at about 1.6 M $(NH_4)_2SO_4$ were dialyzed against H_2O before being further purified on a MonoS® using a LiCl gradient (0–1 M) in 30 mM MES, 1 mM DTT pH 5.8. Proteins that were eluted around 100 mM LiCl were concentrated onto Macrosep Filtron 10 000 then onto Minicon 10 000 (Amicon, Epernon, France), and desalted on PD10 column (Pharmacia) with 50 mM Na_2HPO_4/NaH_2PO_4, pH 7.0, without DTT. The protein was concentrated at 20 mg ml^{-1} and stored at 0°C. The purified ETs conserved their ability to induce the Nikolsky's sign when injected subcutaneously into newborn mice.

Enzymatic assays

Caseinolytic assays were performed in 10 mM Tris-HCl, 150 mM NaCl, 1 mM DTT, pH 8.0 at 37°C. Fluorescein-labeled casein (Sigma) and ETs were used at 480 μg/ml and 100 μg/ml, respectively. After 30 min, 2 h, 4 h or 8 h, macromolecules contained in 400 μl aliquots were pelleted by centrifugation with 1% (w/v) trichloracetic acid for 10 min at 0°C. The supernatant (350 μl) was neutralized by adding 150 μl of 0.2 M Tris-HCl pH 8.0 before the measurement of absorbance at 490 nm. Proteolysis assays in 0.2 M KH_2PO_4 pH 7.8 were done on lapsed lots of insulin (Lilly, France) and human growth hormone (Kabivitrum, Noisy le Grand, France) for 4 h at 37°C, then analyzed on a PHAST® system (Pharmacia) using 20% polyacrylamide gels. For esterolytic activities, Boc–L-Glu–OPhenyl (Sigma) was prepared in dry 1-4 dioxane (Aldrich) as a 500 mM solution and assayed on a DU-40 spectrophotometer (Beckman). Esterolytic activity or NaOH hydrolysis of the substrate was determined by using a molar absorption coefficient of 1.5 mM^{-1} cm^{-1} at 270 nm [44]. At 30°C, the K_m, v_i, V_{max}, k_{cat} values were measured by using 0.5 to 5mM of substrate at 37°C in 500 μl assays containing 1% 1-4 dioxane (v/v) and 2 μg of each ETs, according to Michaelis–Menten kinetics. Among several buffers, such as 0.2 M KH_2PO_4/Tris pH 7.8, 0.05 M Bicine pH 7.8, 0.05 M Hepes pH 7.3, KH_2PO_4 0.2 M pH 7.8 with and without 2 mM $CaCl_2$, only the hepes buffer, with or without $CaCl_2$, gave the most accurate kinetics. Other substrates, Boc–Ala–Ala–Pro–Glu–pNA (where pNA is *p*-nitroanilide), Boc–L-Glu–pNA, Boc–L-Asp–OPhenyl, Boc–L-Glu–OPhenyl and anthranilyl–Ala–Phe–Ala–Phe–Glu–Val–Phe–nitro–Tyr–Asp (Sigma), were tested in the same conditions as above.

Site-directed mutagenesis

Site-directed mutagenesis of the ETA gene inserted in M13mp19 [45] was carried out as previously described [20]. Mutations were sequenced [46] before ETA mutated genes were inserted into the Gram (–)/Gram (+) pCU1 shuttle vector [47] by a *Hind*III-*Hind*III restriction. Vectors containing mutated genes were used for electrotransformation [20] of *S. aureus* RN4220 (*r*– *m*+ *agr*–), and then of *S. aureus* 8325-4 (*r* + *m* + *agr* +), which efficiently expresses the ETA gene.

Crystallization

Initial crystallization conditions were found by screening different precipitation agents. The best crystals were grown at 4°C by vapor diffusion against a reservoir containing 18% PEG 4000, 50 mM sodium phosphate buffer pH 7.0. For the final setup, 5 ml of reservoir solution were mixed with 4 ml of protein solution (initial concentration of 17.7 mg/l) and 1 ml of DMSO. Crystals grow after few days as thin plates. Crystal quality was improved by a new purification scheme described above. Initial diffraction analysis showed twinning problems for some crystals. Subsequently, diffraction data were carefully examined in order to use only single crystals for complete data collection. Wild type ETA, mutants S195C and S147C were crystallized in the same conditions and belong to the same space group.

Data collection

X-ray diffraction data were collected at 4°C on 18 cm Mar-Research image plates and with a Siemens 2D area detector. Laboratory data were collected on a Rigaku rotating anode generator with graphite

monochromator. Synchrotron data for the native were collected at the wiggler station W32 of the Laboratoire pour l'Utilisation du Rayonnement Electromagnetique (LURE), Orsay, France. A native data set between 27 Å and 1.7 Å resolution was obtained by merging a high resolution data set (nat1) collected at LURE and a low resolution data set (nat2) data set collected in the laboratory. For the synchrotron data set (nat1), 243 frames of 0.8° oscillation were collected between 15 Å and 1.7 Å resolution from one crystal. The nat2 data set was collected between 27 Å–3.1 Å resolution; scaling of the two sets was done using data in the resolution range 6 Å–3.5 Å (R_{merge} = 3.5% between the two data sets, calculated on F). After scaling, the final native data were made of reflections from nat1 in the resolution range 6 Å–1.7 Å and of reflections from nat2 in the resolution range 27 Å–6 Å. The final native data set was 99% complete between 27 Å–1.7 Å (57 263 reflections). Data sets were processed with the programs DENZO and SCALEPACK [48] (for image plates data), XDS [49] (for area detector data).

Phasing

Heavy atom binding sites were determined by difference Patterson and Fourier difference maps. Four derivatives (Mersalyl, $KAuCl_4$, EtHgCl, DiHgCl) have a common binding site on each molecule which corresponds to the serine protease active site – (Ser195(195), Asp120(102), His72(57). Refinement of the heavy-atom parameters was performed by the maximum likelihood approach as coded in the programs MLPHARE and SHARP [50,51]. The calculated phases gave an overall figure of merit of 0.622 for data between 27 Å–3.3 Å resolution (SHARP statistics). The 3.3 Å map was improved by solvent flattening, solvent flipping, histogram matching and non-crystallographic symmetry averaging with the programs DM [52] and SOLOMON [53]. All crystallographic calculations were carried out with programs in the CCP4 package [50].

Model building and crystallographic refinement

The modified 3.3 Å resolution MIR map allowed chain tracing for most parts of the polypeptide chain, and a polyalanine model of the ETA molecule was built using the graphics program O [54]. Phases obtained by combining MIR phases with those derived from the polyalanine model using the program SIGMAA [24] were then modified at 3.3 Å resolution, and extended to 2.7 Å by solvent flattening, solvent flipping, histogram matching and non-crystallographic symmetry averaging. This phase modification process combined with model building was repeated several times. The amino acid sequence could be fitted unambiguously for most of the chain to give an initial model which included all 242 residues per monomer. The model was refined with the program X-PLOR [55], using the Engh and Huber stereochemical parameters [56]. Initially, only 3 Å resolution data were included for rigid body refinement followed by torsion-angle refinement. The crystallographic R factor for the starting model was 41.8%. A random sample containing 7% of the data was excluded from the refinement and used for monitoring the course of the refinement [57]. Torsion-angle refinement at 3 Å was followed by rounds of model building in cross-validated Sigmaa-weighted maps with coefficients ($2F_o–F_c$) and ($3F_o–2F_c$) [25,58] and by torsion angle refinement, in which the maximum resolution of the data was gradually increased. Beyond 2.5 Å, the refinement of the atomic parameters was alternated with the refinement of the atomic temperature factors. When the R factor had dropped to 23%, water molecules were added at positions with density higher than 5σ in the $F_o–F_c$ Sigmaa weighted map and compatible with the $2F_o–F_c$ Sigmaa weighted map. Simulated annealing (heating up to 4000°K) using 1.7 Å data was followed by conventional positional and B-factor refinement. All rebuilding and graphic operations were done with O and related Uppsala's programs. At every stage, models resulting from a refinement round were subjected to critical quality analyses, using the programs O, OOPS [59], PROCHECK [60] and WHATIF [61,62].

The refined model

The current model contains two molecules each of 242 residues and includes 417 ordered water molecules. Although the difference between the two molecules in the asymmetric unit were carefully watched during model building, refinements were done without non-crystallographic restraints. Nevertheless, the rms deviation between the Cα atoms of the two monomers in the asymmetric unit is only 0.267Å (the average displacement is 0.196 Å). The quality of the refined structure was assessed using the Biotech validation suite for Protein structures [63]. All residues, except Leu217(220) of each monomer are in the allowed regions of the Ramachandran diagram. Leu217(220) due to its central position in a γ-turn has unusual (φ,ψ) parameters; the electron density for this residue is well-defined (real space correlation factor 0.934 and 0.937 for the two independent molecules) in the ($2F_o–F_c$) cross-validated Sigmaa-weighted map.

Accession numbers

The atomic coordinates have been deposited at the Brookhaven Protein Data Bank with the code 1agj.

Note added in proof

An independent structure determination of the exfoliative toxin A, in another space group at 2.1 Å resolution (Vath, G.M., *et al*., Ohlendorf, D.H. (1997). The structure of the superantigen exfoliative toxin A suggests a novel regulation as a serine protease. *Biochemistry* **36**, 1559–1566), was published after our paper was submitted. As can be judged from both papers, the two structures are similar.

Acknowledgements

We would like to thank Daniel Keller for skillful technical assistance during ETA purification and Pr. Gotz (Tubingen) for providing plasmid pCU1. The authors are indebted to Raymond Ripp for preparation of the figures and to Jean-Marie Wurtz for sequence alignments. We would also like to thank the referees for their very constructive remarks.

References

1. Melish, M.E. & Glasgow, L.A. (1970). The staphylococcal scalded skin syndrome: development of an experimental model. *N. Engl. J. Med.* **282**, 1114–1119.
2. Melish, M.E. & Glasgow, L.A. (1971). The staphylococcal scalded skin syndrome: the expanded clinical syndrome. *J. Pediatr.* **78**, 958–967.
3. Ritter, V.R. (1878). Die exfoliative dermatitis jüngerer Säulinge. *Cent. Z. Kinderheilkd.* **2**, 3–23.
4. Wuepper, K.D., Dimond, R.L. & Knutson, D. (1975). Study of the mechanism of epidermal injury by a staphylococcal epidermolytic toxin. *J. Invest. Dermatol.* **65**, 191–200.
5. Howells, C.H.L. & Jones, E.H. (1961). Two outbreaks of neonatal skin sepsis caused by *Staphylococcus aureus. Arch. Dis. Child.* **36**, 214–216.
6. Kaplan, M.H., Chmel, H., Hsieh, H.C., Stephens, A. & Brinsko, V. (1986). Importance of exfoliatin toxin A production by *Staphylococcus aureus* strains isolated from clustered epidemics of neonatal pustulosis. *J. Clin. Microbiol.* **23**, 83–91.
7. Opal, S.M., Johnson-Winegar, A.D. & Gross, A.S. (1988). Staphylococcal scalded skin syndrome in two immunocompetent adults caused by exfoliatin B-producing *Staphylococcus aureus. J. Clin. Microbiol.* **26**, 1283–1286.
8. Farell, A.M., Ross, J.S., Unasankar, S. & Bunker, C.B. (1996). Staphylococcal scalded skin syndrome in an HIV-1 seropositive man. *Brit. J. Dermatol.* **134**, 962–965.
9. Arbuthnott, J.P., Kent, J., Lyell, A. & Gemmell, C.G. (1971). Toxic epidermal necrolysis produced by an extracellular product of *Staphylococcus aureus*. *Brit. J. Dermatol.* **85**, 145–149.
10. Kapral, F.A. & Miller, M.M. (1971). Product of *Staphylococcus aureus* responsible for the scalded-skin syndrome. *Infec. Immun.* **4**, 541–545.
11. O'Toole, P.W. & Foster, T.J. (1987). Nucleotide sequence of the epidermolytic toxin A gene of *Staphylococcus aureus. J. Bacteriol.* **169**, 3910–3915.
12. Lee, C.Y., Schmitt, J.J., Johnson, W.A.D., Spero, L. & Iandolo, J.J. (1987). Sequence determination and comparison of the exfoliative toxin A and toxin B genes from *Staphylococcus aureus. J. Bacteriol.* **169**, 3904–3909.
13. Piémont, Y., Rasoamananjara, D., Fouace, J.M. & Bruce, T. (1984). Epidemiological investigation of exfoliative toxin-producing *Staphylococcus aureus* strains in hospitalized patients. *J. Clin. Microbiol.* **19**, 417–420.

14. Sato, H., Matsumori, Y., Tanabe, T., Saito, H., Shimizu, A. & Kawano, J. (1994). A new type of staphylococcal exfoliative toxin from a *Staphylococcus aureus* strain isolated from a horse with phlegmon. *Infec. Immun.* 62, 3780–3785.
15. Sato, H., Tanabe, T., Kuramoto, M., Tanaka, K., Hashimoto, T. & Saito, H. (1991). Isolation of exfoliative toxin from *Staphylococcus hyicus* and its exfoliative activity in the piglet. *Vet. Microbiol.* 27, 263–275.
16. Takiuchi, I., Kawamura, M., Teramoto, T. & Higuchi, D. (1987). Staphylococcal exfoliative toxin induces caseinolytic activity. *J. Infec. Dis.* 156, 508–509.
17. Bailey, C.J. & Redpath, M.B. (1992). The esterolytic activity of epidermolytic toxins. *Biochem. J.* 284, 177–180.
18. Dancer, C.J., Garatt, R., Saldnha, J., Jhotti, H. & Evans, R. (1990). The epidermolytic toxins are proteases. *FEBS Lett.* 268, 129–132.
19. Redpath, M.B., Foster, T.J. & Bailey, C.J. (1991). The role of the serine protease active site in the mode of action of epidermolytic toxin of *Staphylococcus aureus*. *FEMS Microbiol. Lett.* 65, 151–155.
20. Prévost, G., Rifai, S., Chaix, M.L. & Piémont, Y. (1991). Functional evidence that the Ser-195 residue of staphylococcal exfoliative toxin A is essential for biological activity. *Infec. Immun.* 59, 3337–3339.
21. Kakudo, S., Yoshikawa, K., Tamaki, M., Nakamura, E. & Teraoka, H. (1992). Secretory expression of a glutamic-acid-specific endopeptidase (Spase) from *Staphylococcus aureus* ATCC12600 in *Bacillus subtilis*. *Appl. Microbiol. Biotechnol.* 38, 226–233.
22. Choi, Y., Kotzin, B., Herron, L., Callahan, J., Marrack, P. & Kapler, J. (1989). Interaction of *Staphylococcus aureus* toxin 'superantigens' with human T cells. *Proc. Natl. Acad. Sci. USA* 86, 8941–8945.
23. Zollner T.H., *et al.*, & Kaufmann, R. (1996). The superantigen exfoliative toxin induces cutaneous lymphocytes-associated antigen expression in peripheral human T lymphocytes. *Immunol. Lett.* 49, 111–116.
24. Read, R.J. (1986). Improved Fourier coefficients for maps using phases from partial structures with errors. *Acta Cryst. A* 42, 140–149.
25. Kleywegt, G.J. & Brünger, A.T. (1996). Checking your imagination. Applications of the free R value. *Structure* 4, 897–904.
26. Perona, J.J. & Craik, C.S. (1995). Structural basis of substrate specificity in the serine proteases. *Protein Sci.* 4, 337–360.
27. Lesk, A.M. & Fordham, W.D. (1996). Conservation and variability in the structures of serine proteinases of the chymotrypsin family. *J. Mol. Biol.* 258, 501–537.
28. Read, R.J. & James, M.N. (1988). Refined crystal structure of *Streptomyces griseus* trypsin at 1.7 Å resolution. *J. Mol. Biol.* 200, 523–551.
29. Hodel, A., Simonson, T., Fox, R.O. & Brünger, A.T. (1993). Conformational substates and uncertainty in macromolecular free energy calculations. *J. Phys. Chem.* 97, 3409–3417.
30. Schiltz, M., Fourme, R., Broutin, I. & Prangé, T. (1995). The catalytic site of serine proteinases as a specific binding cavity for xenon. *Structure* 3, 309–316.
31. Brady, L., *et al.*, & Menge, U. (1990). A serine protease triad forms the catalytic centre of a triaglycerol lipase. *Nature* 343, 767–770.
32. Winkler, F.K., D'Arcy, A. & Hunziker, W. (1990). Structure of human pancreatic lipase. *Nature* 343, 771–774.
33. Brzozowski, A.M., *et al.*, & Thim, L. (1991). A model for interfacial activation in lipases from the structure of a fungal lipase–inhibitor complex. *Nature* 351, 491–494.
34. Schechter, I. & Berger, A. (1967). On the size of the active site in proteases. I. Papain. *Biochem. Biophys. Res. Commun.* 27, 157–162.
35. Barbosa, J.A., Saldanha, J.W. & Garatt, R.C. (1996). Novel features of serine protease active sites and specificity pockets: sequence analysis and modelling studies of glutamate-specific endopeptidases and epidermolytic toxins. *Protein Eng.* 9, 591–601.
36. Nienaber, V.L., Breddam, K. & Birktoft, J.J. (1993). A glutamic acid specific serine protease utilizes a novel histidine triad in substrate binding. *Biochemistry* 32, 11469–11475.
37. Stennicke, H.R., Birkhoft, J.J. & Breddam, K. (1996). Characterization of the S1 binding site of the glutamic acid-specific protease from *Streptomyces griseus*. *Protein Sci.* 5, 2266–2275.
38. Breddam, K. & Meldam, M. (1992). Substrates preferences of glutamic acid-specific endopeptidases assessed by synthetic peptide substrates based on intramolecular fluorescence quenching. *Eur. J. Biochem.* 206, 103–107.
39. Gentilhomme, E., Faure, M., Piémont, Y., Binder, P. & Thivolet, J. (1990). Action of staphylococcal exfoliative toxins on epidermal cell cultures and organotropic skin. *J. Dermatol.* 17, 526–532.
40. Marrack, P. & Kappler, J.W. (1990). The staphylococcal enterotoxins and their relatives. *Science* 248, 705–711.
41. Fleischer, B. & Bailey, C.J. (1992). Recombinant epidermolytic (exfoliative) toxin A of *Staphylococcus aureus* is not a superantigen. *Med. Microbiol. Immunol.* 180, 273–278.
42. Inoue, M., Plantz, G.E. & Shu, S. (1996). Treatment of intracranial tumors by systemic transfer of superantigen-activated tumor-draining lymph node T cells. *Cancer Res.* 56, 4702–4708.
43. Su, Y.-C. & Wong, A.C.L. (1995). Identification and purification of a new staphylococcal enterotoxin, H. *Appl. Environ. Microbiol.* 61, 1438–1443.
44. Houmard, J. (1976). Preparation of chromophoric substrates for the glutamoyl specific staphylococcal protease. *Int. J. Pept. Protein Res.* 8, 199–204.
45. Yanisch-Perron, C., Vieira, J. & Messing, J. (1985). Improved M13 phage cloning vectors and host strains: nucleotide sequences of M13mp18 and pUC19 vectors. *Gene* 33, 103–109.
46. Tabor, S. & Richardson, C.C. (1987). DNA sequence analysis with a modified bacteriophage T7 polymerase. *Proc. Natl. Acad. Sci. USA.* 77, 4761–4771.
47. Augustin, J. & Götz, F. (1990). Transformation of *Staphylococcus epidermidis* and other staphylococcal species with plasmid DNA electroporation. *FEMS Microbiol. Lett.* 54, 203–207.
48. Otwinowski, Z. & Minor, W. (1997). Processing of X-ray diffraction data collected in oscillation mode. *Methods Enzymol.* 276, 307–326.
49. Kabsch, W. (1988). Evaluation of single crystal X-ray diffraction data from a position sensitive detector. *J. Appl. Cryst.* 21, 916–924.
50. Collaborative Computational Project No. 4. (1994). The CCP4 suite : programs for protein crystallography. *Acta Cryst. D* 50, 760–763.
51. De La Fortelle, E. & Bricogne, G. (1997). Maximum-likelihood heavy-atom parameter refinement in the MIR and MAD methods. *Methods Enzymol.* 276, 472–494.
52. Cowtan, K.D. & Main, P. (1993). Improvement of macromolecular electron-density maps by the simultaneous application of real and reciprocal space constraints. *Acta Cryst. D* 49, 148–157.
53. Abrahams, J.P. & Leslie, G.W. (1996). Methods used in the structure determination of bovine mitochondrial F1 ATPase. *Acta Cryst. D* 52, 30–42.
54. Jones, T.A., Zou, J.Y., Cown, S.W. & Kjeldgaard, M. (1991). Improved methods for building protein models in electron density maps and the location of errors in these models. *Acta Cryst. A* 47, 110–119.
55. Brünger, A.T. (1992). X-PLOR, Version 3.1. A system for X-ray Crystallography and NMR. Yale University Press, New Haven, USA.
56. Engh, R.A. & Huber, R. (1991). Accurate bond and angle parameters for X-ray protein structure refinement. *Acta Cryst. A* 47, 392–400.
57. Brünger, A.T. (1992). The free R value: a novel statistical quantity for assessing the accuracy of crystal structures. *Nature* 335, 472–474.
58. Kleywegt, G.J. & Jones, T.A. (1994). Crystal structures of cellular retinoic acid binding proteins I and II in complex with all-trans-retinoic acid and a synthetic retinoid. *Structure* 2, 1241–1258.
59. Kleywegt, G.J. & Jones, T.A. (1996). Efficient rebuilding of protein structures. *Acta Cryst. D* 52, 829–832.
60. Laskwoski, R.A., MacArthur, M.W., Moss, D.S. & Thornton, J.M. (1993). PROCHECK: a program to check the stereochemical quality of protein structures. *J. Appl. Cryst.* 26, 283–291.
61. Vriend, G. (1990). WHATIF: a molecular modelling and drug design program. *J. Mol. Graphics* 8, 52–56.
62. Vriend, G. & Sander, C. (1993). Quality control of protein models : directional atomic contact analysis. *J. Appl. Cryst.* 26, 47–60.
63. Wodak, S.J., Pontius, J., Vaguine, A. & Richelle, J. (1995). Validating protein structures. From consistency checking to quality assessment. In *Proceedings of the CCP4 Daresbury Study Weekend:* "*Making the most of your model*", pp. 41–51, SERC Daresbury Laboratory, Warrington, UK.
64. Evans, S.V. (1993). SETOR: hardware lighted three-dimensional solid model representations of macromolecules. *J. Mol. Graphics* 11, 134–138.
65. Moult, J., Sussman, F. & James, M.N. (1985). Electron density calculations as an extension of protein structure refinement. *Streptomyces griseus* protease at 1.5 Å resolution. *J. Mol. Biol.* 182, 555–566.
66. Read, R.J., Fujinaga, M., Sielecki, A.R. & James, M.N. (1983). Structure of the complex of *Streptomyces griseus* protease B and the third domain of the turkey ovomucoid inhibitor at 1.8 Å resolution. *Biochemistry* 22, 4420–4433.
67. Fujinaga, M., Delbaere, L.T., Brayer, G.D. & James, M.N. (1985). Refined structure of alpha-lytic protease at 1.7 Å resolution. Analysis of hydrogen bonding and solvent structure. *J. Mol. Biol.* 184, 479–502.
68. Hutchinson, E.G. & Thornton, J.M. (1996). PROMOTIF: A program to identify and analyze structural motifs in proteins. *Protein Sci.* 5, 212–220.
69. Barton, G.J. (1993). ALSCRIPT: a tool to format multiple sequence alignments. *Protein Eng.* 6, 37–40.